

**Original Research Article****Removal of Calcium over Apricot Shell Derived Activated Carbon: Kinetic and thermodynamic study**Alaa MT Al-Layla^{1,*} , Abdelrahman B. Fadhil²¹*Department of Chemistry, College of Science, Mosul University, Mosul, Iraq*²*Laboratory Researches of Industrial Chemistry, Department of Chemistry, College of Science, Mosul University, Mosul, Iraq***ARTICLE INFO****Article history**

Submitted: 2021-09-11

Revised: 2021-09-25

Accepted: 2021-10-17

Manuscript ID: CHEMM-2109-1380

Checked for Plagiarism: Yes

Language Editor:

Dr. Behrouz Jamalvandi

Editor who approved publication:

Dr. Hasan Karimi-Maleh

DOI: 10.22034/CHEMM.2022.1.2

KEY WORDS

Apricot shells

Activated carbon

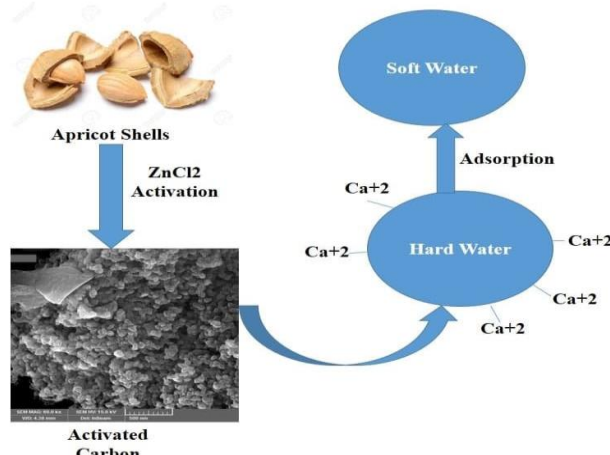
Hardness

Adsorption

Adsorption isotherms and kinetics

ABSTRACT

The apricot shells (AS) derived activated carbon (AC) was employed in removing the water hardness ions (calcium) from synthetic hard water. The $ZnCl_2$ activation route was implemented in synthesizing the AC from the AS. The typical AC sample was diagnosed for its morphology by the FESEM technique, elemental analysis using EDX technique, influential surface groups by FTIR spectroscopy, and crystallinity by the XRD. This AC sample was then applied to eliminate the calcium ion (Ca^{+2}) from synthetic hard water by investigating factors affecting the Ca^{+2} removal efficiency, like the solution pH, Ca^{+2} initial concentration, AC dosage, temperature, and contact time. The outcomes revealed that Ca^{+2} removal by the so-synthesized AC is pH, temperature, and time-dependent. The best Ca^{+2} removal % reached 80.12 %, while the best adsorption capacity was 70.42 mg/g. The Langmuir adsorption isotherm and the pseudo-second-order kinetic model demonstrated were best described Ca^{+2} removal by the AC. The enthalpy and Gibbs free energy functions indicated that Ca^{+2} adsorption is endothermic and spontaneous. Thus, the consequences assured that the ASs derived AC can be exploited as an effective adsorbent to remove Ca^{+2} from the solution.

GRAPHICAL ABSTRACT

* Corresponding author: Alaa MT Al-Layla

✉ E-mail: alaa.mt.allayla@uomosul.edu.iq

© 2022 by SPC (Sami Publishing Company)

Introduction

Among the most known impurities, which cause water pollution are the ions of both magnesium (Mg) and calcium (Ca). The presence of the ions salts of these elements in water results in water hardness (WH). The WH is a scale to specify the amount of the divalent ions, like Mg^{+2} and Ca^{+2} in water. When rocks containing these ions are in contact with the groundwater, these ions will dissolve in it and make it hard [1-2]. Water contains hardness ions with a level above 300 ppm is not useful for the domestic uses [3]. As a result of their occurrence in the earth strata, the Ca, Mg, and carbonate ions affect the groundwater's hydrochemistry [4]. The reaction of humidity and CO_2 gas with Ca and Mg ions occur on the surface of the earth form water hardness (WH) [5]. WH is divided into two classes, temporary and permanent; the former can be removed through boiling, and the latter needs special treatment for removal [6]. The presence of hardness ions in water (tap, river, and ground) is associated with many drawbacks, such as induction of scaling harms, significant problems in boilers and pipelines, hair and skin toughening, reducing the cleaning action of detergents. Also, the occurrence of the hardness ions in water diminishes the heat transfer in the boiler, the creation of precipitates, which decrease the flow rate, staining both clothes and dishes, and affecting the action of washing machines, steam irons, and dishwashers as well [3,7-11]. Many techniques have been employed to eliminate these ions from the HW, such as lime-soda, microbial, ion exchange process, chemical precipitation, nano-filtration, electro deionization process, evaporation, and adsorption [13-15]. The latter is a promising and widely applied technique due to its cost efficiency, fast, and economic process for removing heavy metal ions from contaminated waters [16]. Numerous adsorbents were employed in the HW softening, like zeolites [17], waste tires rubber ash [18], resins (cationic and anionic) [19], and carbon-based adsorbents [7,9,13,20-22]. Implementing the active carbon (AC) as an effective adsorbent has been established in the literature as an outcome of its porous structure, elevated capacity of adsorption,

and the occurrence of varied functional groups onto its surface, which is a typical adsorbent for varied applications including softening of hard HW [21]. Diverse carbon-based materials were implemented in the preparation of the AC including coal, petroleum residue, lignite, and waste polymers [23,24]. Nevertheless, these carbon-based materials are exhausted and costly. Therefore, biomass wastes are possible carbon-based sources for the synthesis of AC as they are costless, available, and renewable [25]. On this account, various bio-wastes, such as de-oiled seed cakes [26], hazelnut shell [27], coconut shell [28], corn cob [29], cherry seeds [30], date pits [31], and apricot seeds [32] were examined as costless raw materials for the creation of AC to lessen its production cost. These bio-wastes are suitable precursors for AC preparation due to their chemical compositions, which consist essentially of cellulose, lignin, and hemicellulose. These constituents contain varied functional groups, like methoxy, hydroxyl, carboxyl, phenols, etc, which contribute to the effective removal of diverse contaminants from wastewaters [33]. Also, the ratio of these ingredients varies greatly from a precursor to another. Apricot belongs to stone fruits, which follows the *Rosaceae* family under the *Prunoidae* family and the *Prunus* gender. It is one of the most essential fruits as a result of its high economical and nutritional value. It is also rich in Vitamin A. In 2012, the average production of apricot amounted 3956640 tons. Turkey is the leader in apricot production (795768 tons), followed by Iran (460000 tons). The number of the apricot trees in Iraq reached 917501 with an average production of 26276 tons of apricot. Each apricot tree produces about 28.60 kg of apricot [34]. Apricot stone, which is a lingo-cellulosic material, possesses the features vital for the synthesis of AC. Apricot stones derived activated carbons were employed in the purification of wastewaters from diverse organic and inorganic pollutants [25,35]. However, the utilization of the AC synthesized from apricot shells by the $ZnCl_2$ activation method for the elimination of Ca^{+2} from its aqueous solution has not been addressed in the literature as far as our knowledge goes. The adsorption performance of Ca^{+2} by the AS derived

AC using $ZnCl_2$ as an activating agent was the essential objective of this investigation. The adsorption isotherms and kinetics of Ca^{+2} onto the as-synthesized AC was also inspected.

Materials and Methods

Experimental

As the precursor, apricot shells (AS) were provided from the local agricultural markets during the summer of 2019. Chemicals, such as Iodine, solution 0.05 mol/l (0.1 N), Sodium thiosulfate, solution 0.1 mol/l (0.1 N), Starch solution 1% w/v, sodium hydroxide ($NaOH$, 98.0%), Hydrochloric acid, solution 1 mol/l (1 N), calcium carbonate ($CaCO_3$, 98.0 – 100.5 %), and zinc chloride ($ZnCl_2$, 98.0 – 100.5 %) were provided from Scharlab (Scharlab, Barcelona, España).

Analysis of the AS

The AS were analyzed for their ultimate and proximate analysis. The proximate analysis of the AS was accomplished following the ASTM 3174 and ASTM 3175 to identify its contents of volatiles, humidity, ash, and fixed carbon. A Variael CUBE, Germany, CHNSO elemental analyzer, was employed to specify the ultimate analysis of the AS. The method suggested by [36] was exploited in identifying the component analysis of the AS.

Synthesis of the AC

The AS were thoroughly washed by water to eliminate foreign materials, such as dust, dried under sunlight for two days, crushed by a heavy-duty electrical grinder, and finally sieved by a 60-mesh sieve. In the preparation of the AC, the dried AS were soaked in solutions contain different amount of $ZnCl_2$. The mixture was left overnight to assure the total wetting of the AS by the $ZnCl_2$ solutions. Next, the impregnated samples were heated in an oven at 105°C until dryness. The dried impregnated samples were finally placed in a quartz tube followed by pyrolysis by means of a tubular furnace. The resulted AC was then immersed in a 0.1M HCl solution for a day to throw away the remains of $ZnCl_2$, followed by washing with warm distilled water until getting a neutral water. To finish, drying the AC was done at 105°C for 24h at and finally maintained in a preserved container for the subsequent use [36,37].

The synthesis of the AC samples was accomplished through four series including investigating the effect of the impregnation ratio (0.5:1 to 3:1 $ZnCl_2$:AS), temperature of activation (400-800 °C), activation period (30-120 minutes), and particle size of the feed (30, 40, 60 and 70 mesh) on the iodine number (IN) as well as the AC yield. The IN of the AC samples was specified as per AATM 1112-01, 2006 standard test method.

Identification of AC

The as-synthesized AC was characterized by several techniques. The surface morphology of the AC was identified through Field Emission Scanning Electron Microscopy (FESEM) on a TESCAN MIRA FESEM and Zeiss EVO MA10 series coupled with EDX, Czech Republic. The Energy Dispersive X-Ray Fluoresces (EDX) technique was employed in the determination of the elemental analysis of the AC. The IN of the AC samples was specified as per AATM 1112-01, 2006 standard test method. The surface functional groups on the AC were distinguished by Fourier transform infrared spectroscopy (FTIR) with a FTIR JASCO V-630, USA in the range of 4000 to 400 cm⁻¹. A Malvern Panalytical X-ray diffraction (XRD), UK, was implanted in determining the XRD patterns of the so-synthesized AC utilizing Cu-K α radiation at a static scanning for 2θ value in a range of 10°–80°.

Adsorption experiments of Ca^{+2}

The Ca^{+2} batch adsorption experiments were accomplished through agitating a given mass of the AC with 50 mL of Ca^{+2} solution of desired concentration and pH at 35 °C and 200 rpm in a thermo-stated shaker. When the equilibrium was attained, the amount of Ca^{+2} adsorbed by the AC was specified by a flam photometer. Effect of pH in the range of 2-11 on the Ca^{+2} removal by the as-created AC was investigated by adjusting the solution pH by either a 0.10 M solution of $NaOH$ or HCl. A HANNA pH meter was employed indenturing the solutions pH was inspected. The influence of the Ca^{+2} initial concentration (50-300 ppm), AC dose (0.05-0.3 g), temperature (35 °C, 45 °C, and 55 °C), and contact period (30-240 minutes) on the adsorption efficiency of Ca^{+2} by the AC was instigated. The percentage removal

(R%) of Ca^{+2} by the AC was calculated as follows (Equation 1):

$$R(\%) = \frac{(C_0 - q_e)}{C_0} \times 100 \quad 1$$

where, C_0 and C_e (mg/L) are respectively the initial and equilibrium liquid-phase concentrations of Ca^{+2} . The amount of Ca^{+2} adsorbed per 1g of the AC was specified as follows (Equation 2):

$$q_e = \frac{(C_0 - q_e)V}{W} \quad 2$$

where V (L) is the volume of solution and W (g) is the AC mass utilized in the adsorption experiment. The Langmuir and Freundlich isotherms were employed to inspect the adsorption equilibrium of Ca^{+2} . Also, the adsorption data of Ca^{+2} was analyzed by the pseudo-first-order and pseudo-second-order kinetics.

Table 1: Elemental, proximate, and component analysis of the AS

Elemental analysis (wt.%)	AS
C%	47.10
H%	6.22
O%	46.37
N%	0.31
H/C molar ratio	1.58
O/C molar ratio	0.73
Empirical formula	$\text{CH}_{1.58}\text{N}_{0.005}\text{O}_{0.73}$
Proximate analysis (wt.%)	AS
Moisture	7.33
Fixed carbon %	15.88
Volatiles %	75.91
Ash %	0.88
Lignocellulosic composition (wt. %)	AS
Cellulose	29.02
Hemicellulose	15.44
Lignin	48.55
Extractives	6.99

The percentages of lignin, cellulose, and hemicellulose in the feedstock affect the AC porosity. It was established that as an outcome of its raised stability besides little reactivity, lignin could endure the activation process's destructive reactions. On this account, the fixed carbon content in the precursor relates to its content of lignin, which is principally in charge of the AC carbon skeletons and aids in developing its porous-structure [39]. Hemicellulose and cellulose are volatile constituents and essentially accountable for the formation of AC with meso and macro-porosity [40]. In conclusion, the AS can be employed as a potential feedstock for AC creation because of its high lignin content.

Result and Dissection

Composition of the AS

It is evident from Table 1 displaying the elemental, proximate, and component analysis of the AS, that the latter could be a potential feedstock for AC preparation. The outcomes given in Table 1 revealed that the ash content in the AS was below that fixed for bagasse and rice husk [38]. This outcome is very significant for the precursor utilized in AC preparation. The fixed carbon for the AS was greater than that of bagasse and comparable to that established for rice husk [38]. However, biomass with high content of the volatile matters and good yield of fixed carbon is useful as a feedstock for the preparation of AC [37].

Synthesis of the AC from AS

Figure 1a discloses that the AC yield increased with the low ZnCl_2 impregnation % and then dropped as the impregnation % of ZnCl_2 exceeded 1.0 ZnCl_2 : feedstock. As generally established, the carbonization process of lignocellulosic precursors is accompanied by the liberation of O and H in the form of H_2O , CH_4 , CO , CO_2 , tar, and aldehydes. Thus, at the low impregnation % of ZnCl_2 , the raw material dehydration in the form of H_2O and H_2 occurs. However, this depends on the carbon content of the parent precursor. When higher impregnation % of the ZnCl_2 was utilized, the yield declined due to further burn-off of the precursor into CO , CO_2 , CH_4 , and tar, leading to a

lower AC yield. Similar outcomes have also been established during the AC synthesis from cattle-manure Compost [41], Soybean straw [42], and Fox nutshell [43] utilizing the same activating agent. The AC samples exhibited an increased IN values at the lower impregnation % of ZnCl₂ due to forming a microporous structure in the AC samples. While the impregnation % of ZnCl₂ exceeded the optimal ratio, the IN diminished as a result of the extra burn-off of the carbon and the widening of microspores into mesopores [37]. The functional groups present onto the AC surface besides its textural structures and physical and chemical features are dramatically influenced by the activation temperature. A progressive diminish in the AC yield was beholden as the temperature of activation rose, as demonstrated in Figure 1b, due to the precursor's further devolatilization and dehydration. It was shown by Rodriguez-Reinoso [44] that three stages are involved during the activation process. The first stage involves opening of primary inaccessible pores, while the creation of new orifices via further selective activation occurs upon the

second stage. Widening of the created new pores occurs in the final stage. It is evident from Figure 1b that raising the activation temperature above the optimum ones declined the AC yield due to the further loss of the volatile ingredients. These findings were also beholden by Demiral *et al.* [45] during the synthesis of AC from the pumpkin seed shells by the ZnCl₂ activation method. Figure 1b demonstrates that the SA of the synthesized AC samples enhanced with further raising of temperature. This result may be ascribed to the additional elimination of volatiles as temperature of activate rises, resulting in the creation of new micro-pores. On this account, 600 °C exhibited the ideal IN, while temperatures beyond 600°C diminished the IN as an outcome of micro-pores walls damage, giving a rise to micro-pores widening into meso and macro-pores [42]. AC synthesis from pumpkin seed shells utilizing the same activating agent exhibited similar outcomes [45]. The activation period influence on both AC yield and IN was investigated by testing various periods of activation (20-120 minutes) at 600°C, as apparent in Figure 1c.

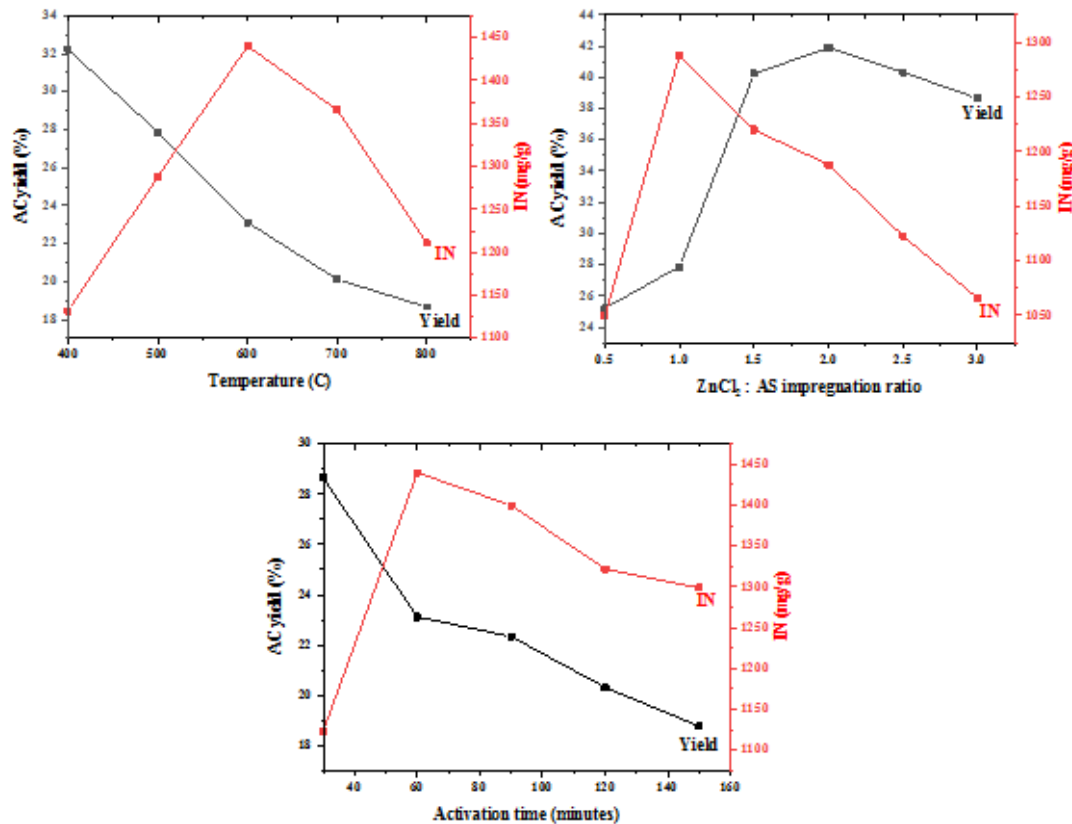


Figure 1: Effect of (a) ZnCl₂ impregnation ratio, (b) activation temperature, and (c) activation period on the AC yield and AC

The outcome revealed that the AC yield dropped as the time of activation increased from 20 to 120 minutes. This result may be attributed to the fact that the prolonged period of activation is accompanied by an additional dehydration of the precursor, leading to a lower yield. The IN of the AC samples was enhanced with prolonging of the activation period as a reason of forming new micro-pores on the AC surface due to the extra dehydration of the feedstock. Yet, the IN of the AC dropped when the time of activation exceeded the best period. This reduction may be ascribed to the distortion or expansion of the micro-pores into mesopores against the adsorption of iodine [43]. The same results were also reported by Sahin *et al.* [46] upon the $ZnCl_2$ activation of *Elaeagnus Angustifolia* seeds, respectively, to create AC.

Identification of the AC from AS

FESEM image of the AC, which is demonstrated in Figure 2, visualizes its surface morphology. FESEM image of the AC exhibited that it owns roughly texture with heterogeneous surface and a diversity of randomly distributed pore size. Also, it possessed an irregular and highly porous surface, suggesting relatively high surface area. These observations have also supported by the IN value and SA of the AC. The pore development is the outcome of the reaction of the activating agent with precursor components upon the activation process. The rough surface of the AC and its irregular pores are formed as an outcome of $ZnCl_2$ evaporation upon the carbonization process [47].

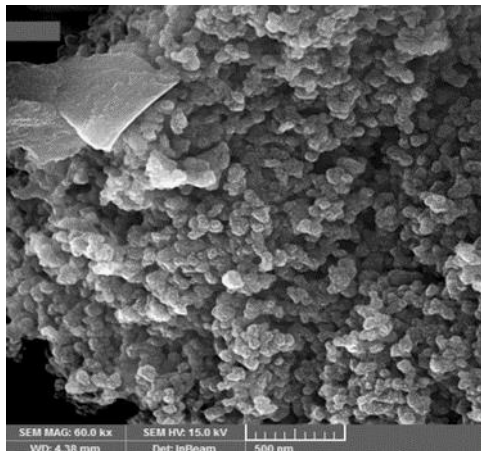


Figure 2: The SEM image of the AC from AS

The XRD pattern of the so-created AC sample, which is illustrated in Figure 3, is referred to the occurrence of two broad diffraction signals situated at $2\theta = 26^\circ$ and 45° attribute to (002) and

(100) phases. The broadness of the XRD peaks specifies the slight crystallinity of as-attained AC sample [48].

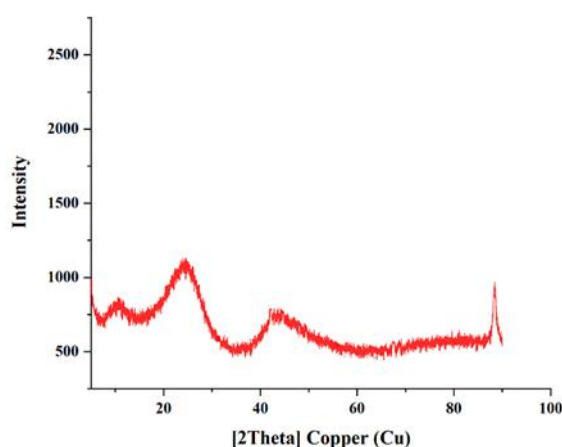


Figure 3: The XRD pattern of the AC from AS

The FTIR spectrum of the as-obtained AC was specified in the range of 400-4000 cm⁻¹, as illustrated in Figure 4. The wide band observed in the range of 3600-3000 cm⁻¹ is attributed to the (O-H) stretching vibration originated from phenols, alcohols, and the absorbed water. The absorption peaks observed in the range of 2922-2853 cm⁻¹ were ascribed to the asymmetric and symmetric of the (-C-H) group. The absorption peak corresponded to the (C=O) group stretching vibration in an aldehyde, esters, carboxylic acid, and ketone was seen at 1633 cm⁻¹. The absorption peaks in the range of 1685-1570

cm⁻¹ may have originated from the overlapping bands of highly conjugated carbonyls, C=C and C=N stretching vibrations in the aromatic ring. The bands between 1600 cm⁻¹ and 1437 cm⁻¹ could be ascribed to the vibrations of the aromatic ring in the AC sample. The peak at 1389 cm⁻¹ is attributed to the (-C-H) stretching vibration. The band at 1117 cm⁻¹ is attributed to the (C-O) stretching vibration. The observed absorption peaks have also been seen in the AC sample prepared through carbonization of various biomass wastes using ZnCl₂ [49,50].

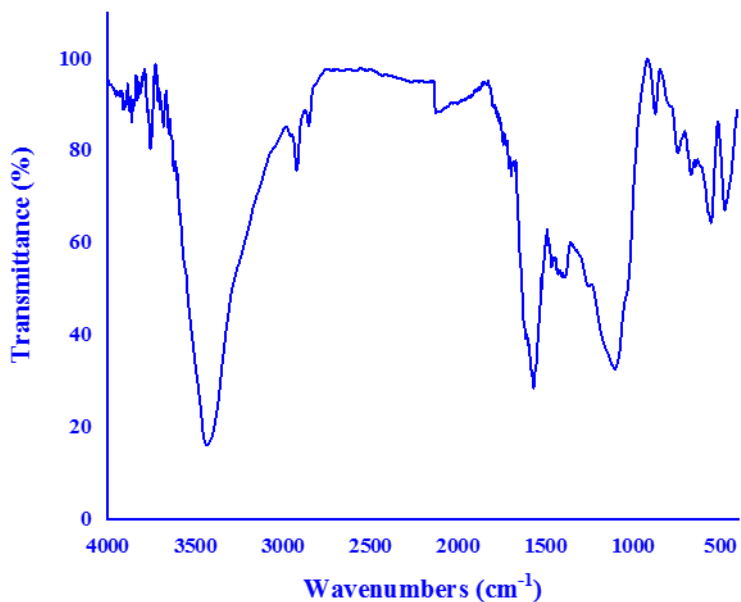


Figure 4: The FTIR spectrum of the AC from AS

Figure 5 The EDS image of the so-prepared AC sample. It can be seen from Figure 5 that carbon and oxygen are the main elements forming the AC.

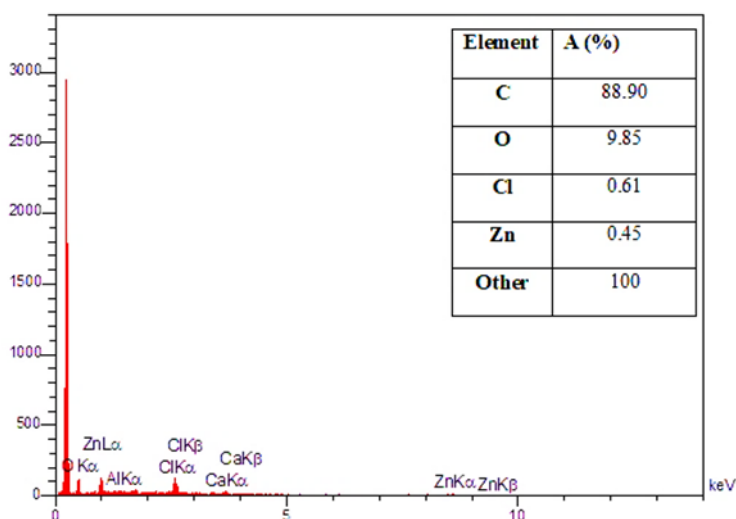


Figure 5: The EDS image of the AC from AS

Factors affecting the adsorption experiments of Ca⁺² ions

The active interface between the adsorbent and adsorbate can be greatly influenced by the initial

pH value of solution. Accordingly, the impact of the initial pH of the solution was inspected as seen in Figure 6a. Following the FTIR spectra outcomes, the AC surface contains diverse effective groups, such as the aliphatic hydroxyl, phenolic, and carboxyl occurred. These effective functional groups aid in the removal of Ca^{+2} ions from water through either ion exchange mechanism or by the electrostatic attraction with these groups [51]. As per the outcomes illustrated in Figure 6a, the adsorption of Ca^{+2} ions onto the AC surface increased with raising the solution pH. This result suggests that at pH lower than 2, the pH of the AC surface will be greater than that of the solution. Thus, the positively charged onto the AC surface will cause an electrostatic repulsion between the Ca^{+2} ions and the surface of the AC. Thus, the elimination of Ca^{+2} ions will mainly proceed through the ion exchange mechanism, and thereby, the adsorption of Ca^{+2} ions did not happen [51]. This phenomenon happens due to the fact that under the low pH, a competition between capturing H^+ and Ca^{+2} ions occurs, which in turn declines taking up more amount of Ca^{+2} ions. Also, a large quantity of H_2O molecules would be adsorbed when the hydrophilicity of the AC is high, which leads to the occupation of the adsorption site and hinders the adsorption of Ca^{+2} ions [51]. Increasing the solution pH was accompanied by an increment in the adsorption of Ca^{+2} ions. Raising the solution pH from 2 to 10 results in a complete adsorption of the Ca^{+2} ions thorough ion exchange with the positively charged functional groups onto the AC surface. When the solution pH became an alkaline, the AC surface will be negatively charged. This will lead to an increasing induction of the electrostatic attraction between the AC and the Ca^{+2} ions, resulting in a significant enhancement in the adsorptive capacity of the AC. On this account, a pH of 10 was the typical value for Ca^{+2} adsorption onto the as-created AC.

The influence of the Ca^{+2} primary concentration on its adsorptive removal by the so-created AC was inspected by testing solutions with different concentrations (100–300 mg/L). The experiments were conducted using 0.10 g of the AC, pH=10 at 30 °C for 300 minutes.

Figure 6b demonstrate that the quantity of Ca^{+2} eliminated by the AC was enhanced as the initial concentration of the solution was raised. An initial concentration of 200 mg/L exhibited the highest amount of Ca^{+2} adsorbed. Beyond this concentration, no further adsorption occurred. This outcome can be ascribed to the fact that as there are vacant adsorption sites onto the AC surface, the chemisorption of the Ca^{+2} increases with increasing the Ca^{+2} initial concentration. Later on, the sites will be occupied by the Ca^{+2} ions, the further increase in the Ca^{+2} initial concentration will not enhance the adsorbed amount of the Ca^{+2} [52].

The impact of the AC dosage on the uptake of Ca^{+2} ions was studied over various amount of the AC in the range of (0.05 – 0.30 g), as demonstrated in Figure 6c, with keeping pH, temperature, initial concentration, and contact time fixed at 10,30C,200 mg/L, and 300 minutes, respectively. The Ca^{+2} uptake increased as the AC dosage increased. The best adsorption of Ca^{+2} was acquired at an AC dosage of 0.20 g. Beyond this dosage, the Ca^{+2} adsorption declined. This outcome is ascribes to increasing the AC dosage over the optimal dosage that will result in an agglomeration in some AC particles, making the AC surface inaccessible for adsorption, resulting in a lower adsorption capacity [53].

Metal ions elimination from aqueous solution is temperature-reliant. Thus, the impact of temperature on Ca^{+2} elimination by the so-prepared AC was inspected through conducting many experiments at various temperatures (10 °C - 50 °C), while preserving other factors, including pH, contact time, AC dosage, and Ca^{+2} initial concentration is fixed at 10,300 minutes, 0.20 g, and 200 mg/L, respectively.

As depicted in Fig. 6d, the Ca^{+2} amount adsorbed by the AC increased with raising temperature, suggesting the indicating endothermic nature of Ca^{+2} sorption processes [54,55]. Another reason is that raising temperature influences the contact between the sorbent and metal ions, which in turn affects the stability of the metal-sorbent complex. Furthermore, sorption of metal ions enhances with raising temperature because of the increment of the solute kinetic energy as well as

the surface activities. In general, rising of temperature enhances the sorbate diffusion rate through the exterior boundary layer and the

interior pores of the sorbent particles. Thus, more active sites will be ready to adsorb more hardness ions with raising temperature [7,54].

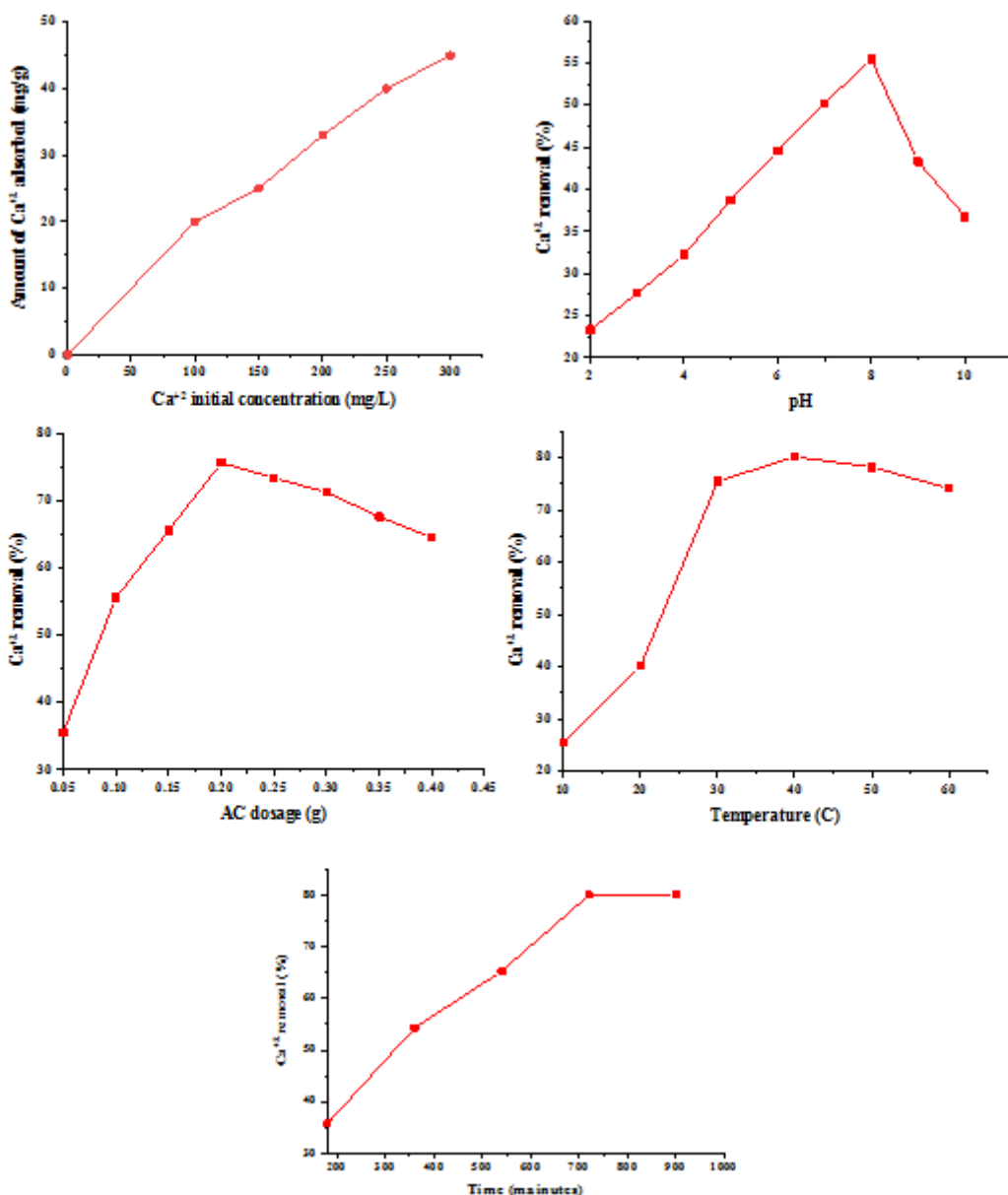


Figure 6: Impact of (a) pH, (b) initial concentration of Ca^{+2} solution, (c) AC quantity, (d) temperature, and (e) contact period on the Ca^{+2} adsorptive removal %

The Ca^{+2} elimination efficiency by the so-created AC was inspected through trying various durations upon the adsorption process ranges (60-360 minutes) with fixing other factors fixed at their ideal values. Figure 6e clarifies that that extending the adsorption time was accompanied by an improvement in the removal efficiency of Ca^{+2} from solution. Primarily, the Ca^{+2} adsorption process was fast, and then reduced by 180 minutes. The equilibrium was attained after 300 minutes. Increasing the removal % of Ca^{+2} before attaining the equilibrium is ascribed to the fact

that at the first stages of the adsorption, the sorbent effective centers are vacant and ready for adsorption. With extending time, number of the effective binding sites declined, resulting in a lower removal process as a consequence of the complete occupation of the sorbent surface with the Ca^{+2} ions [55].

Adsorption isotherms

Information related to the sorbent capacity as well as the interaction nature between the sorbent-sorbate can be provided through adsorption isotherms. Besides, constants from the adsorption

isotherms are necessary to deduce the highest adsorption uptake besides describing the sorbent affinity and the surface features [55]. The Langmuir model of adsorption, which supposes the formation of a monolayer layer onto the sorbent homogenous surface, is expressed in Equation 3, as follows:

$$\frac{C_e}{q_e} = \frac{1}{q_m K_L} + \frac{C_e}{q_m} \dots \dots \dots \quad 3$$

where q_m denotes the supreme sorbent monolayer capacity (mg/g), while K_L relates to the Langmuir

constant of adsorption (L/mg). A linear relationship (Figure 7a) can be obtained when C_e/q_e is plotted against C_e/q_m in which its slope gives the q_m and the intercept gives the K_L . The adsorption favorability can be deduced from the separation factor (R_L), obtained from Equation 4:

$$R_L = \frac{1}{1+C_0 K_L} \quad 4$$

Based on the R_L value, which is ($0 < R_L < 1$), the Ca^{+2} sorption by the so-obtained AC is favorable.

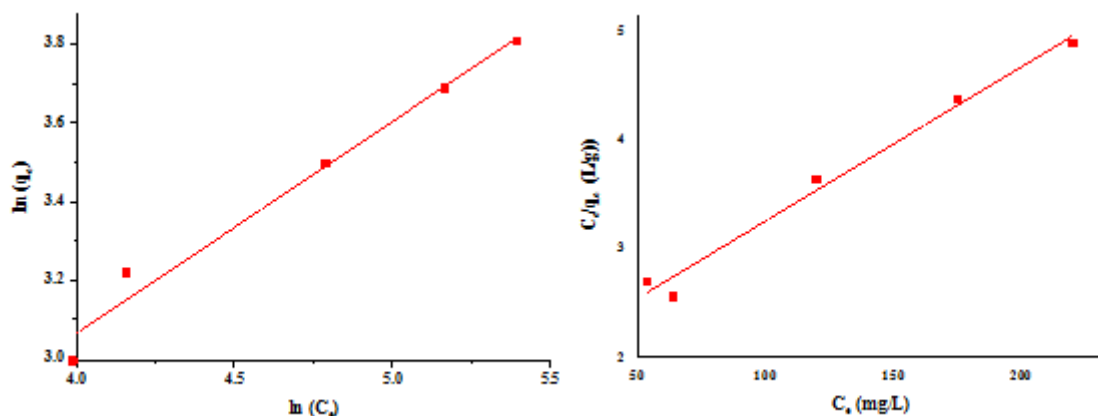


Figure 7: (a) The Langmuir linear isotherm and (b) the Freundlich isotherm of Ca^{+2} adsorption by the AS derived AC

The Freundlich model of the sorption isotherms suggests the sorbent besides the sorbate multi-layer coverage. Equation 5 expresses the linear form of the Freundlich model of sorption isotherms:

$$\ln q_e = \ln K_F + \frac{1}{n} \ln C_e \dots \dots \quad 5$$

From this equation, the Freundlich constants K_F (mg/g), which relates to adsorption capacity (mg/g), can be obtained from the plot's slope, while n , which gives information about sorption intensity (g/L), can be obtained from the plot's

intercept (Figure 7b). To know if the sorption is favorable, the value of n ought to be above 1.0. In this study, the Ca^{+2} adsorption by the AC is satisfactory because the value of n was above 1.0. Based on the results given in Table 2, the Langmuir isotherm described best the Ca^{+2} adsorption by the as-obtained AC compared with the Freundlich isotherm. This outcome was drawn from the relatively higher R^2 value ($R^2=0.9709$) for the Langmuir isotherm than that of the other model.

Table 2: The Langmuir and Freundlich constants

Langmuir adsorption isotherm			
$q_m (\text{mg/g})$	$K_L (\text{L/mg})$	R_L	R^2
71.42	0.0079	0.3361	0.9912
Freundlich adsorption isotherm			
n	$K_F (\text{mg/g})$	R^2	
1.92	1.10	0.9742	

Kinetic of Ca^{+2} adsorption by the AC

The Ca^{+2} adsorption kinetics onto the AS derived AC was inspected by analyzing the adsorption

outcomes based on the pseudo-first-order and pseudo-second-order models of kinetics, as respectively illustrated in Figures 8a and 8b.

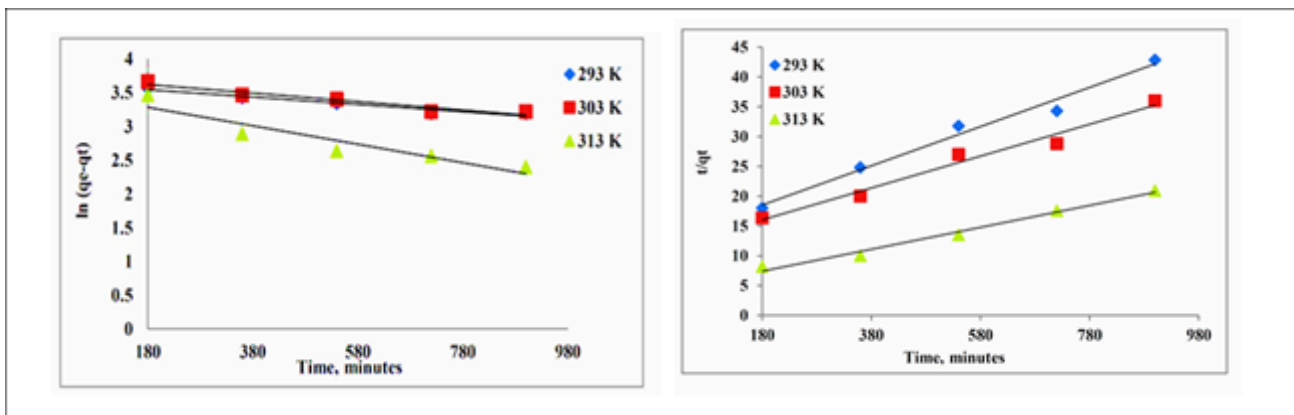


Figure 8: (a) The pseudo-first-order and (b) the pseudo-second-order models of kinetics of Ca^{+2} adsorption by the AS derived AC

The kinetic experiments were inspected at a temperature range of 303 -323 K. The kinetic model consequences revealed that the pseudo-second-order model described better the Ca^{+2} adsorption by the as-prepared AC as the consequence of the higher R^2 value for the pseudo-second-order than the one observed by the pseudo-first-order. As the Ca^{+2} adsorption

outcomes followed the pseudo-second-order model, chemisorption is supposed to be the rate-limiting step, suggesting that the interaction between the Ca^{+2} ions and the AC surface are either by charge neutralization or electrostatic attraction [33,54]. Table 3 offers the constants relate to pseudo-first-order model and pseudo-second-order model.

Table 3: The pseudo-first-order and pseudo-second-order models of kinetics constants

Temperature (K)	Pseudo-first-order-model		
	k_1	$q_e (\text{mg/g})$	R^2
293	0.00054	1.29	0.9447
303	0.00063	2.41	0.9275
313	0.0013	1.25	0.8729
Pseudo-second-order model			
Temperature (K)	k_2	$q_e (\text{mg/g})$	R^2
303	0.000085	30.42	0.9809
313	0.00006	38.46	0.9750
293	0.00007	55.55	0.9863

Adsorption thermodynamics

Thermodynamics functions (ΔH , ΔS , and ΔG) of Ca^{+2} adsorption by the AC from AS at 300 mg/L initial concentration of Ca^{+2} were specified by batch studies at numerous temperatures (303 K, 313 K, and 323 K). Calculating thermodynamic functions was accomplished using the following equations [33]:

$$\ln\left(\frac{q_e}{C_e}\right) = \frac{\Delta S_0}{R} + \frac{\Delta H_0}{RT} \dots \dots \quad 7$$

$$\left(\frac{q_e}{C_e}\right) = K \dots \dots \quad 8$$

$$\Delta G_0 = -RT \ln K \dots \dots \quad 9$$

where, ΔS_0 (kJ.mol^{-1}), ΔH_0 (kJ.mol^{-1}), ΔG_0 (kJ.mol^{-1}), and K , are the standard change in entropy, change in enthalpy, and Gibbs free energy, and the equilibrium coefficient, respectively. The liner plot of $1/T$ vs. $\ln q_e/C_e$ yields the ΔH_0 and ΔS_0 , which could be determined respectively from the plot slope and intercept. The thermodynamic functions values presented in Table 4 clearly indicated that the adsorption of Ca^{+2} by the as-created AC was endothermic ($\Delta H_0 = 0.6982 \text{ kJ.mol}^{-1}$), indicating that the Ca^{+2} adsorption by the AC is temperature-dependent. Also, the adsorption of Ca^{+2} by the AC was spontaneous as a result of negative value of ΔG_0 .

Table 4: The pseudo-first-order and pseudo-second-order models of kinetics constants

ΔH_o (kJ.mol ⁻¹)	ΔS_o (kJ.mol ⁻¹)	ΔG_o (kJ.mol ⁻¹)		
		293 K	303 K	313 K
0.6982	0.02	- 7.11	- 6.68	- 5.70

Fixed bed ADS results

The adsorptive elimination of the Ca⁺² from aqueous solution by the so-created AC was also achieved through a fixed bed system, and the obtained results indicated that the sample's flow rate through the column significantly affected the R%. The best Ca⁺² elimination through a fixed-bed system was 77.55 % at 10 drops/min rate of flow, followed by 15 drops/min (71.21%) and 20 drops/min (66.56 %). More contact between the Ca⁺² molecules and the AC particles occurred at the slower flow rate, resulting in better removal efficiency. Compared with the stirring method, the Ca⁺² elimination % by the fixed-bed system was slightly below that obtained via the stirring process. Also, the fixed-bed system consumed a long time to reach the maximum Ca⁺² elimination % compared with the stirring process. This outcome may be ascribed to the fact that stirring increases the collisions among the Ca⁺² ions and the AC particles, resulting in a better Ca⁺² removal%.

Conclusion

This investigation showed that the AC synthesized via ZnCl₂ activation route produced an AC sample with 23.12 % yield and 1440 mg/g iodine adsorption number utilizing 1:1 ZnCl₂:AS impregnation ratio, 500 °C temperature of activation, and 60 minutes period of activation. The adsorptive efficiency of the so-created AC suggests its suitability for eliminating Ca⁺² from synthetic hard water with a removal efficiency of 80.12% and adsorption capacity of 71.42 mg/g using 100 ml of 300 mg/L calcium solution at 40 °C for a contact period of 720 minutes using 0.20 g of the AC at a pH value of 10.0. The Ca⁺² from synthetic hard water fitted best to the Langmuir model of adsorption isotherms and the pseudo-second-order rate model of kinetics. These results were deduced from the high regression index value (R²) of these models compared with other adsorption isotherms and kinetics models. The so-

synthesized AC can be employed successfully in hard water treatment.

Acknowledgments

Authors would like to express their sincere thanks to Mosul University, College of Science, Chemistry Department for providing facilities to carry out this work.

Funding

This research did not receive any specific grant from funding agencies in the public, commercial, or not-for-profit sectors.

Authors' contributions

All authors contributed toward data analysis, drafting and revising the paper and agreed to be responsible for all the aspects of this work.

Conflict of Interest

We have no conflicts of interest to disclose.

ORCID

Alaa MT Al-Layla:

<https://www.orcid.org/0000-0002-2061-1461>

References

- [1]. Kannan D., Mani N., *Asian J. Res. Chem.*, 2019, **12**:248. [[Crossref](#)], [[Google Scholar](#)], [[Publisher](#)]
- [2]. Agostinho L.C.L., Nascimento L., Cavalcanti B.F., *Open Access Sci. Rep.*, 2012, **1**:1 [[Crossref](#)], [[Google Scholar](#)], [[Publisher](#)]
- [3]. Hailu Y., Tilahun E., Brhane A., Resky H., Sahu O., *Groundw. Sustain. Dev.*, 2019, **8**:457 [[Crossref](#)], [[Google Scholar](#)], [[Publisher](#)]
- [4]. Tirkey, P., Bhattacharya, T., Chakraborty S., Baraiik, S., *Groundw. Sustain. Dev.*, 2017, **5**:85 [[Crossref](#)], [[Google Scholar](#)], [[Publisher](#)]
- [5]. Boyd C.E., Tucker C.S., Somridhivej B., *J. of the Worl. Aquacul. So.*, 2016, **47**:6 [[Crossref](#)], [[Google Scholar](#)], [[Publisher](#)]
- [6]. MacAdam J., Jarvis P., *Water-formed scales and deposits: types, characteristics, and relevant*

- industries. Mineral Scales and Deposits, Elesiver, 2015 [[Crossref](#)], [[Google Scholar](#)], [[Publisher](#)]
- [7]. Varada K., *Int. J. Life Sci.*, Special Issue .2018: 1 [[PDF](#)]
- [8]. Rolence C., Machunda R.L., Njau K.N., *Sci. Technol. Soc.*, 2014, **2**:97 [[Crossref](#)], [[Google Scholar](#)], [[Publisher](#)]
- [9]. Lestari A.Y.D., Sukirman A.M., Ilmi, M.I., Sidiq M., *MATEC Web Conf.*, 2018, **154**:10 [[Crossref](#)], [[Google Scholar](#)], [[Publisher](#)]
- [10]. Seo S.J., Jeon H., Lee J.K., Kim G.Y., Park D., Nojima H., Lee J., Moon S.H., *Water Res.*, 2010, **44**:2267 [[Crossref](#)], [[Google Scholar](#)], [[Publisher](#)]
- [11]. WHO, Hardness in Drinking-water Background Document for Development of WHO: Guidelines for Drinking-water Quality. WHO Press. 2011
- [12]. Tofighy M.A., Mohammadi T., *Desalination*, 2011, **268**:208 [[Crossref](#)], [[Google Scholar](#)], [[Publisher](#)]
- [13]. Zhang Z., Chen A., *Sep. Purif. Technol.*, 2016, **164**:107 [[Crossref](#)], [[Google Scholar](#)], [[Publisher](#)]
- [14]. Ouar, M.L.A., Sellami M.H., Meddour S.E., Touahir R., Guemari S., Loudiyi K., *Groundw. Sustain. Dev.*, 2017, **5**:261 [[Crossref](#)], [[Google Scholar](#)], [[Publisher](#)]
- [15]. Cretescu I., Soreanu, G., Harja M., *Int. J. Environ. Sci. Technol.*, 2015, **12**:1799 [[Crossref](#)], [[Google Scholar](#)], [[Publisher](#)]
- [16]. Song J., Liu M., Zhang Y., *AIChE J.*, 2020, **61**:640 [[Crossref](#)], [[Google Scholar](#)], [[Publisher](#)]
- [17]. Saad S., Amjad L., Hamad A., *Revista AUS.*, 2016, 1 [[PDF](#)]
- [18]. Aghakhani A.S.F., Mousavi B., Mostafazadeh-Fard R., Seraji R.M., *Desalination*, 2011, **275**:217 [[Crossref](#)], [[Google Scholar](#)], [[Publisher](#)]
- [19]. Rostamian R., Heidarpour M., Mousavi S.F., Afyuni M., *Adv. Environ. Biol.*, 2014, **12**:202 [[Google Scholar](#)]
- [20]. Li G., Shang J., Wang Y., Li Y., Gao H., *J. Environ. Sci.*, 2013, **25**:S101 [[Crossref](#)], [[Google Scholar](#)], [[Publisher](#)]
- [21]. Mestre A.S., Nabiço A., Figueiredo P.L., Pinto, M.L.S., Santos C.S., Fonseca I.M., *Chem. Eng. Sci.*, 2016, **286**:538 [[Crossref](#)], [[Google Scholar](#)], [[Publisher](#)]
- [22]. Saleem J., Shahid U.B. Hijab M., Mackey H., McKay G., *Biomass Convers. Biorefin.*, 2019, **9**:775 [[Crossref](#)], [[Google Scholar](#)], [[Publisher](#)]
- [23]. Ayoob A.K., Fadhil A.B., *Fuel*, 2020, **264**:116754 [[Crossref](#)], [[Google Scholar](#)], [[Publisher](#)]
- [24]. Caoa J., Wub Y., Jina Y., Yilihana P., Yang S., *Desalination Water Treat.*, 2015, **53**:2990 [[Crossref](#)], [[Google Scholar](#)], [[Publisher](#)]
- [25]. Aldobouni I.A., Fadhil A.B., Saied I.K., *Energy Sources A Recovery Util. Environ. Eff.*, 2015, **37**:2617 [[Crossref](#)], [[Google Scholar](#)], [[Publisher](#)]
- [26]. Lewicka K., *Pol. J. Chem. Technol.*, 2017, **2**:38 [[Crossref](#)], [[Google Scholar](#)], [[Publisher](#)]
- [27]. Yusmartini E.S., Setiabudaya D., Syarofi R., Faizal M., *Adv. Mat. Res.*, 2014, **896**:149 [[Crossref](#)], [[Google Scholar](#)], [[Publisher](#)]
- [28]. Tang S., Chen Y., Xie R., Jiang W., Jiang Y., *Water Sci. Technol.*, 2016, **73**:2654 [[Crossref](#)], [[Google Scholar](#)], [[Publisher](#)]
- [29]. Angin D., *Fuel*, 2014, **115**:804 [[Crossref](#)], [[Google Scholar](#)], [[Publisher](#)]
- [30]. Darweesh T.M., Ahmed M.J., *Ecotoxicol. Environ. Saf.*, 2017, **138**:139 [[Crossref](#)], [[Google Scholar](#)], [[Publisher](#)]
- [31]. Jankovi B., Mani N., Dodevski V.D., Radovi I., Pijovi M., *J. Clean. Prod.*, 2019, **236**:117614 [[Crossref](#)], [[Google Scholar](#)], [[Publisher](#)]
- [32]. Namal O.O., Kalipci E., *Int. J. Environ Anal. Chem.*, 2019 **100**:1 [[Crossref](#)], [[Google Scholar](#)], [[Publisher](#)]
- [33]. İncedayıl B., Tamer E.C., Sinir G.O., Suna S., Çopur O.U., *Food Sci. Technol.*, 2017, **36**:273 [[Crossref](#)], [[Google Scholar](#)], [[Publisher](#)]
- [34]. Mansora A.M., Lima J.S., Anib F.N., Hashima H., Hoa W.S., *Chem. Eng.*, 2019, **72**:79. [[Crossref](#)], [[Google Scholar](#)]
- [35]. Hidayu A.R., Muda N., *Procedia Eng.*, 2016, **148**:106 [[Crossref](#)], [[Google Scholar](#)], [[Publisher](#)]
- [36]. Fadhil A.B., Nayyef A.W., Sedeeq S.H., *Asia-Pac J. Chem. Eng.*, 2021, **15**:e2390 [[Crossref](#)], [[Google Scholar](#)], [[Publisher](#)]
- [37]. Boonpoke A., Chiarakorn S., Laosiripojana, N., Towprayoon S., Chidthaisong A., *J. Sust. Energy Environ.*, 2011, **2**:77 [[Google Scholar](#)], [[Publisher](#)]
- [38]. Correa R.C., Stollovsky M., Hehr T., Rauscher Y., Rolli B., Kruse A., *ACS Sustain. Chem. Eng.*, 2017, **9**:8222 [[Crossref](#)], [[Google Scholar](#)], [[Publisher](#)]

- [39]. Hong D., Zhou J., Hu C., Zhou Q., Mao J., Qin Q., *Fuel*, 2019, **235**:326 [[Crossref](#)], [[Google Scholar](#)], [[Publisher](#)]
- [40]. Qian Q., Machida M., Tatsumoto H., *Bioresour. Technol.*, 2007, **98**:353 [[Crossref](#)], [[Google Scholar](#)], [[Publisher](#)]
- [41]. Miao Q., Tang Y., Xu J., Liu X., Xiao L., Chen Q., *J. Taiwan Inst. Chem. Eng.*, 2013, **44**:458 [[Crossref](#)], [[Google Scholar](#)], [[Publisher](#)]
- [42]. Kumar A., Jena H.M., *Appl. Surf. Sci.*, 2015, **356**:753 [[Crossref](#)], [[Google Scholar](#)], [[Publisher](#)]
- [43]. Rodriguez-Reinoso F., *Springer: Dordrecht*, 1991, **192**:533. [[Crossref](#)], [[Google Scholar](#)], [[Publisher](#)]
- [44]. Demiral I., Aydin S.C., Demiral H., *Desalin. Water Treat.*, 2016, **57**:2446 [[Crossref](#)], [[Google Scholar](#)], [[Publisher](#)]
- [45]. Şahin Ö., Saka C., Ceyhan A.A., Baytar O., *Sep. Sci. Technol.*, 2015, **50**:886 [[Crossref](#)], [[Google Scholar](#)], [[Publisher](#)]
- [46]. Suat U., Erdem M., Tay T., Karagoz S., *Appl. Surf. Sci.*, 2009, **255**:8890 [[Crossref](#)], [[Google Scholar](#)], [[Publisher](#)]
- [47]. Abo El Naga A.O., El Saied M., Shaban S.A., El Kady F.Y., *J. Mol. Liq.*, 2019, **285**:9 [[Crossref](#)], [[Google Scholar](#)], [[Publisher](#)]
- [48]. He X., Ling P., Yu M., Wang X., Zhang X., Zheng M., *Electrochimica Acta.*, 2013, **105**:635 [[Crossref](#)], [[Google Scholar](#)], [[Publisher](#)]
- [49]. Yagmura E., Gokcea Y., Tekina S., Semercib N.I., Aktasa Z., *Fuel*, 2020, **267**:117232 [[Crossref](#)], [[Google Scholar](#)], [[Publisher](#)]
- [50]. Li G., Shang J., Li Y.W.Y., Gao H., *J. Environm. Sci.*, 2013, **25**:S10 [[Crossref](#)], [[Google Scholar](#)], [[Publisher](#)]
- [51]. Largitte L., Brudey T., Tant T., Dumesnil P.C., Lodewyckx P., *Micropor. Mesopor. Mat.*, 2016, **219**:265 [[Crossref](#)], [[Google Scholar](#)], [[Publisher](#)]
- [52]. Kalak T., Cierpiszewski R., *Pol. J. Chem. Technol.*, 2019, **21**:72 [[Crossref](#)], [[Google Scholar](#)], [[Publisher](#)]
- [53]. Fadhil A.B., Saeed H.N., Saeed L.I., *Asia-Pac. J. Chem. Eng.*, 2021, **16**:1 [[Crossref](#)], [[Google Scholar](#)], [[Publisher](#)]
- [54] Mohammed-Taib B.M., Fadhil A.B., *Inter. J. Envi. Anal. Chem.*, 2021, **1** [[Crossref](#)], [[Google Scholar](#)], [[Publisher](#)]
- [55]. Rattanapan S., Srikram J., Kongsume P., *Energy Procedia.*, 2017, **138**:949 [[Crossref](#)], [[Google Scholar](#)], [[Publisher](#)]

HOW TO CITE THIS ARTICLE

Alaa MT Al-Layla, Abdelrahman B. Fadhil. Removal of Calcium over Apricot Shell Derived Activated Carbon: Kinetic and thermodynamic study, *Chem. Methodol.*, 2022, 6(1) 10-23

DOI: 10.22034/CHEMM.2022.1.2

URL: http://www.chemmethod.com/article_139108.html